NANO LETTERS

2008
Vol. 8, No. 1
183−188

Single-Molecule Detection and Mismatch Discrimination of Unlabeled DNA Targets

Anders Gunnarsson, Peter Jönsson, Rodolphe Marie, Jonas O. Tegenfeldt, and Fredrik Höök*

Department of Physics, Division of Solid State Physics and the Nanometer Consortium, Lund University, Sölvegatan 14, 223 62 Lund, Sweden

Received September 18, 2007; Revised Manuscript Received November 14, 2007

ABSTRACT

We report on a single-molecule readout scheme on total internal reflection fluorescence microscopy (TIRFM) demonstrating a detection limit in the low fM regime for short (30-mer) unlabeled DNA strands. Detection of unlabeled DNA targets is accomplished by letting them mediate the binding of suspended fluorescently labeled DNA-modified small unilamellar vesicles (Ø ∼ 100 nm) to a DNA-modified substrate. On top of rapid and sensitive detection, the technique is also shown capable of extracting kinetics data from statistics of the residence time of the binding reaction in equilibrium, that is, without following neither the rate of binding upon injection nor release upon rinsing. The potential of this feature is demonstrated by discriminating a single mismatch from a fully complementary sequence. The success of the method is critically dependent on a surface modification that provides sufficiently low background. This was achieved through self-assembly of a biotinylated copolymer, Poly(L-lysine)-g-poly(ethylene glycol) (PLL-*g*-PEG) on a silicon dioxide surface, followed by subsequent addition of streptavidin and biotinylated DNA. The proposed detection scheme is particularly appealing due to the simplicity of the sensor, which relies on self-assembly principles and conventional TIRFM. Therefore, we foresee a great potential of the concept to serve as an important component in future multiplexed sensing schemes. This holds in particular true in cases when information about binding kinetics is valuable, such as in single nucleotide polymorphism diagnostics.

During the past decades, the development of ultrasensitive bioanalytical sensors has attracted significant interest. This stems primarily from their high potential to improve biomedical diagnostics, drug discovery, and forensic analysis, but also from the need for advanced bioanalytical assays in fundamental research. Label-free DNA sensing using nanoscale devices based on electrical[1,2] or optical[3,4] target detection has shown great promise in the strive for high sensitivity and specificity. Indeed, different strategies have been shown feasible for detection of unlabeled targets in the low fM regime. Conductance measurements, utilizing silicon nanowires, have been shown capable of detecting short, unlabeled DNA strands in the low fM concentration regime.[5] Other approaches involve various amplification procedures to enhance the signal and thus the detection capacity. Low fM concentrations could be reached with imaging surface plasmon resonance on RNA microarrays using the enzymatic capability of RNase H to remove multiple RNA strands on the surface when hybridized to target DNA.[6] Another equally sensitive strategy involves silver enhancement of surface-immobilized DNA-modified gold nanoparticles, in which case binding to a surface was mediated by unlabeled targets.[7] With few exceptions,[1] previous reported assays compatible with detection of low target concentration rely on end-point measurements, thus excluding information regarding binding kinetics.

Besides mass-transport limitations and parasitic signals generated through unspecific binding events, the major challenge to accomplish reliable detection of low abundant analytes is the sensitivity and acquisition rate of the transducer principle. With single-molecule sensitivity and sufficient suppression of unspecific binding events, the detection limit is essentially set by the affinity of the interaction and the possibility to control mass transport to the site of detection. Indeed, using a sensor concept based on an optical microcavity, the vision of label-free single-molecule detection was very recently verified for low molecular weight (∼15 kD) proteins.[8] In the present paper, we report of an alternative sensor assay capable of detecting single unlabeled low abundant biomolecules, exemplified by detection of short (30 bases) DNA targets. Single-molecule sensitivity was accomplished using total internal reflection (TIR) excitation, in which case the evanescent wave penetrates only a few hundred nanometers into the liquid phase, thus efficiently removing background noise from out-of-focus fluorescent molecules.[9,10] To transfer the hybridization of unlabeled DNA targets to a signal detectable using TIR fluorescence microscopy (TIRFM), binding of DNA-modi-

* Corresponding author. E-mail: fredrik.hook@ftf.lth.se. Tel: (+)46 (0)-46-222 1494. Fax: (+)46 (0)46-222 3637.

10.1021/nl072401j CCC: $40.75
Published on Web 12/19/2007

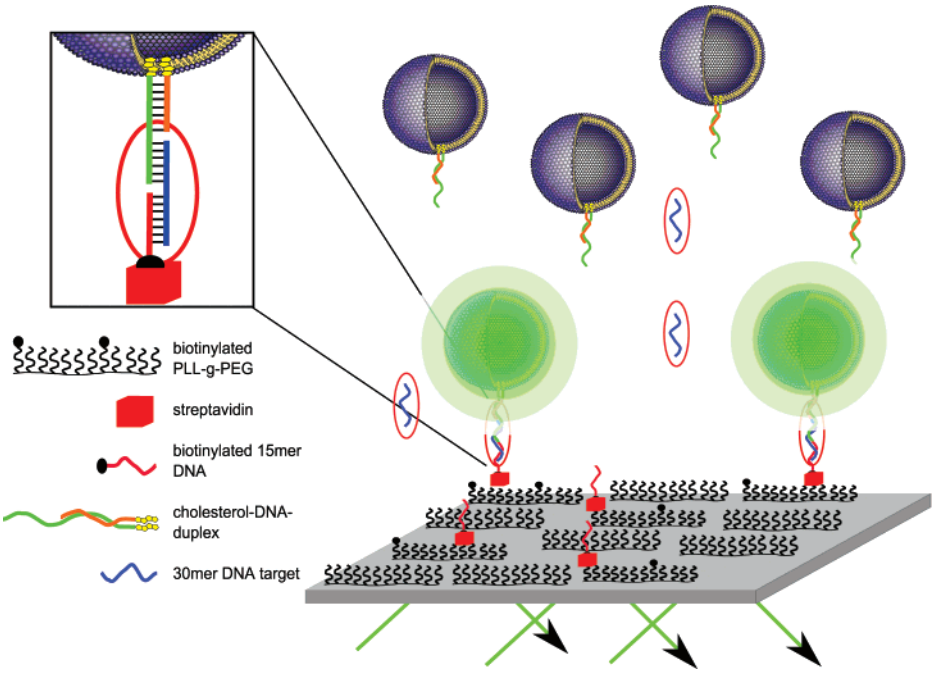

Figure 1. Schematic illustration of the sensing template based on subsequent self-assembly of biotinylated copolymer (PLL-*g*-PEG/PLL-*g*-PEGbiotin), streptavidin, and biotinylated DNA onto the negatively charged silicon dioxide surface. Detection is accomplished by introducing ~100 nm rhodamine-labeled lipid vesicles exposing 15 free-hanging single-stranded DNA bases. The 30 bases single-stranded target hybridizes with both the free-hanging surface-immobilized DNA (15 bases) and the DNA on the vesicles, thereby attracting the vesicle to the surface. Detection is accomplished using TIR excitation of the surface-immobilized vesicles, thereby efficiently reducing background fluorescence from all unbound vesicles in the bulk.

fied fluorescent lipid vesicles to within the evanescent field was ensured to occur in the presence of (unlabeled) DNA targets only. Furthermore, while previous fluorescent or amplification-based DNA detection systems primarily rely on end-point measurements,[7,11] the imaging mode of the TIRFM system not only provides detection of individual DNA targets through continuous counting of individual bound lipid vesicles, but also a new means to extract information about binding kinetics. This is accomplished by monitoring the residence time of the individual vesicles in the bound state. Interestingly, the information obtained from the binding kinetics analysis is shown sufficient to distinguish between different binding reactions, exemplified by efficiently discriminating between specific and unspecific interactions as well as between fully complementary and single mismatch DNA.

Reliable detections of low abundant targets as well as a sufficient contrast in kinetics between different types of interactions require that unspecific binding events are efficiently suppressed. This was accomplished through spontaneous self-assembly of biotinylated PLL-*g*-PEG (PLL-*g*-PEGbiotin) onto a negatively changed silicon dioxide surface, known to be resistant to protein and lipid vesicle adsorption.[12,13] The substrate was further modified with single-stranded DNA (15 bases) by subsequent addition of a biotinylated oligonucleotide conjugated to steptavidin. The fluorescently labeled vesicles were modified with DNA (15-mer), as described previously,[14] allowing unlabeled DNA targets (30-mer) to mediate binding of the easily detectable vesicles to the DNA-modified substrate, as schematically illustrated in Figure 1.

The aqueous-based self-assembly steps used to modify the silicon dioxide substrate, including subsequent additions of DNA-modified lipid vesicles, was verified using quartz crystal microbalance with dissipation monitoring (QCM-D) (E4 instrument, Q-Sense, Sweden), as shown in Figure 2.

The initial decrease in frequency reflects the self-assembly of biotinylated PLL-*g*-PEG (1:1 molar ratio of mixture of PLL-*g*-PEG/PLL-*g*-PEGbiotin) and was followed by a similar response upon addition of biotinylated single-stranded DNA (5′-biotin-ACGTCAGTCTCACCC-3′) conjugated to streptavidin (2:1 molar ratio). Note that the frequency responses from the initial surface modifications (step 1 and 2) are almost identical on all three crystals (red, blue, and green curves), demonstrating a reliable and reproducible surface chemistry. Upon addition of the target strands (5′-TATTTCTGATGTCCAGGGTGAGACTGACGT-3′ (blue) and 5′-CTGAGTGAATATTGTGGGTGAGACTGACGT-3′ (red)) in step 3, there is a decrease in frequency of 8 Hz (red and green curves), which confirms efficient hybridization to the surface-immobilized DNA. After saturated binding in step 3, a free-hanging 15 bases long single-stranded DNA is potentially available for subsequent binding of DNA-modified vesicles.

Vesicles were modified with DNA by incubating a vesicle suspension with hybridized pairs of cholesterol-terminated DNA strands (3′-cholesterol-CCCAGGCAGCACGGAA-TAAAGACTACAGGT-5′ and 5′-cholesterol-CCCTCCGT-CGTGCCT-3′). The two cholesterol moieties ensure strong binding of cholesterol−DNA to the vesicle membrane,[14] and the difference in length of the two strands provides a free-hanging single-stranded overhang, suitable for hybridization

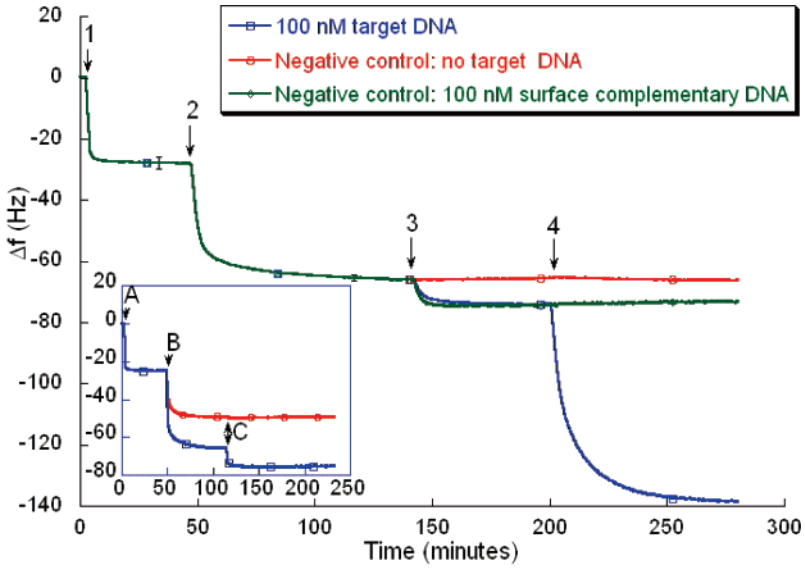

Figure 2. Changes in frequency, Δf, vs time upon sequential exposure of a SiO_2-coated QCM crystal to (1) PLL-*g*-PEG/PLL-*g*-PEGbiotin (1:1 molar ratio, 10 μg/mL), (2) biotinylated 15-mer DNA conjugated to streptavidin (1:2 molar ratio, 100 nM:10 μg/mL), and (3) target DNA, which were complementary to the free-hanging strand on the surface but where the solution-exposed overhang was either complementary (blue) or noncomplementary (red) to the DNA on the vesicles added in step 4. In the experiment represented by the red curve, no addition was made in step 3 and was at (4) followed by addition of DNA-modified vesicles. Inset shows Δf vs time upon addition of (A) PLL-*g*-PEG/PLL-*g*-PEGbiotin, (B) biotinylated 15-mer DNA conjugated to streptavidin (blue) or streptavidin only (red) followed by (C) 100 nM complementary target DNA on both crystals. Parallel measurements of up to four crystals were made, where negative control measurements were run in parallel with target detection.

to the free-hanging part of targets immobilized on the surface. Upon addition of DNA-modified vesicles to the substrate, modified as described above with DNA complementary to the overhang (blue), there is a decrease in frequency of 65 Hz. This is a representative signal for vesicle binding,[13] thus confirming binding of intact tethered vesicles.

To verify that the coupling of DNA-labeled vesicles represents sequence-specific DNA hybridization, a set of negative control experiments were performed. Upon exposure of the DNA-modified surface to DNA-modified vesicles (step 4) in the absence of target DNA (red), no mass uptake was observed. Similarly, in the presence of target DNA complementary to the surface-immobilized strand only, target binding is observed (step 3), but no response is observed upon addition of DNA-modified vesicles (green). Together, this proves the sequence specificity of the sensor concept. Another prerequisite of the assay is that the PLL-*g*-PEG/streptavidin layer effectively suppresses unspecific binding of DNA targets alone. This was tested by exposing the PLL-*g*-PEG/ PLL-*g*-PEGbiotin-modified substrates to DNA targets after incubation with either streptavidin alone (red in inset) or the biotinylated DNA/streptavidin complex used above (blue in inset). While complementary DNA bind readily, no detectable binding was observed for the surface containing streptavidin, thus verifying that the substrate is sufficiently resistant to DNA adsorption.

With this macroscopic verification of the surface chemistry (see Supporting Information for further details), the step to single lipid-vesicle imaging was accomplished using TIRFM. Excitation of fluorophores in close proximity (100−200 nm) to the surface is ensured by the rapidly decaying evanescent electromagnetic wave at the interface between the substrate and the aqueous medium. To ensure that the presence of a fluorescently labeled vesicle within the TIR field is mediated through one DNA target only, the average number of DNA per vesicle was controlled to be lower than one by mixing the bivalent cholesterol-based coupled DNA duplex with vesicles in a 1:10 ratio. In addition, to minimize the probability of two or more DNA strands in close proximity on the surface, the ratio between PLL-*g*-PEGbiotin and PLL-*g*-PEG was reduced to 1:1000. Finally, a sufficiently high signal-to-noise ratio was ensured by adding approximately a thousand fluorophores (1 wt %) each to the DNA-modified lipid vesicles.

Prior to the addition of the vesicle suspension and the TIRF imaging, the surface was exposed for 40 min to the solution containing the target sequence. DNA-target-mediated vesicle binding could be distinguished from nonbinding vesicles, because the latter rapidly disappear from the excitation field or change location after every frame collected by the CCD camera, as illustrated in Figure 3 for the case of 100 fM target DNA (see Supporting Information for full length movies).

Target detection is obtained by distinguishing hybridized vesicles remaining bound for multiple frames (green circles) from noninteracting vesicles that disappear from the surface during the time between two frames (blue circles). Vesicles that are bound for multiple frames, but still detach from the surface prior to the end of the measurement, are shown in red. A custom-made code was written in Matlab (see Supporting Information for details), based on the rules defined above to distinguish bound from unbound vesicles, and used to analyze the movies. The total accumulation of bound vesicles versus time was evaluated for two different target concentrations, as shown in Figure 4. All bleached

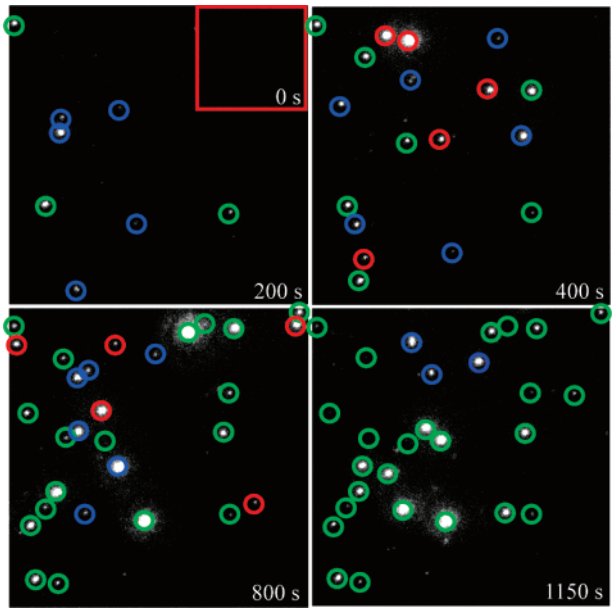

Figure 3. TIRF micrograph snapshots at various times in a movie sequence after introduction of labeled vesicles to a DNA-modified surface pre-exposed to the target DNA. The micrographs illustrate excitation of single vesicles in close proximity to the interface after preincubation of the target sequence (100 fM). Vesicles are highlighted with color-coded rings to visualize the different processes. Green circles indicate vesicles that remain bound to the surface beyond the last frame of the measurement. Red circles highlight vesicles immobilized on the surface for at least ten frames but that are released prior to the last fame of the measurement. Blue circles indicate vesicles only present for less than ten frames. (See Supporting Information for entire filtered and nonfiltered movie sequences). Field of view is 90 × 90 $(\mu m)^2$.

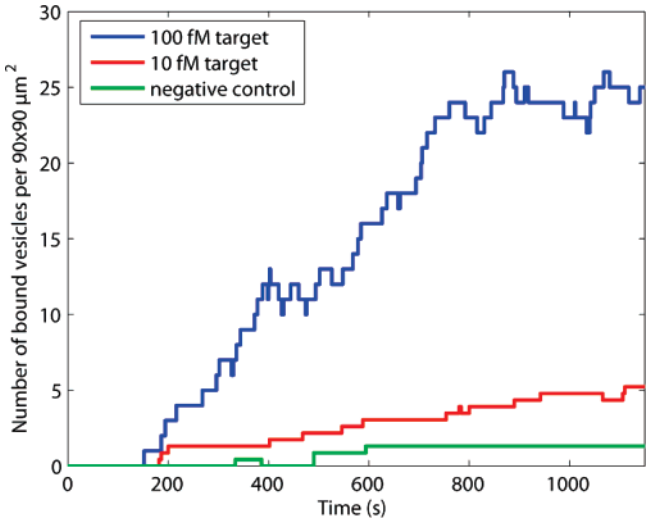

Figure 4. Data extracted from the filtered TIRF movies showing the accumulated number of bound vesicles on a 90 × 90 $(\mu m)^2$ surface area as a function of time. The curves corresponding to the 10 fM target and the negative control were measured with a field of view of 140 × 140 $(\mu m)^2$ and subsequently scaled down to get more reliable values on the surface coverage in these cases. The negative control contains no target DNA. To provide low levels of unspecific binding, the substrate was preincubated with unlabeled vesicles containing noncomplementary DNA.

vesicles are counted as bound for the curves in Figure 4. The results were confirmed by visual inspection.

In Figure 4, note first that virtually zero background was accomplished for the negative control, confirmed by as few as three false detections, on a surface area of 140 × 140 $(\mu m)^2$ during the entire detection time of 20 min. For the field of view (90 × 90 $(\mu m)^2$) used for the images in Figure 3, this corresponds to only one false detection during the entire detection time. This means, in turn, that essentially each vesicle detected in the presence of target DNA corresponds to a single hybridization event. Under such conditions, the detection limit is in principle determined by the affinity constant of the interacting molecules and the fluidics used to control liquid exchange. Without any optimization of the latter, the current detection limit is approximately 10 fM, but this value is expected to be possible to reduce further by improving the surface chemistry to achieve an even lower occurrence of nonspecific binding events and concentration depletion due to binding in tubings, cell walls, etc. Because in principle a single adsorbed vesicle is enough for detection, the nonspecific binding of vesicles is currently what sets the detection limit. Note also that due to the highly limited number of binding sites on the surface, controlled by the high PLL-*g*-PEG/PLL-*g*-PEGbiotin ratio, the assay is expected to be essentially reaction-limited and not influenced by mass-transport limitations. Assuming a Langmuir binding model, the number of bound molecules, n_t, on the surface for a reaction-limited system with low target concentration can be expressed as

$$n_t \propto (C/K_d)(1 - \exp(-t/\tau)) \quad (1)$$

where C is the target concentration in bulk, $K_d = k_{off}/k_{on}$ and $\tau = (k_{on}C + k_{off})^{-1} \approx 1/k_{off}$.

Because the dissociation constant, k_{off}, for the system was determined to be around 0.002 s^{-1} (see below), this means that the binding of vesicles to the surface for a reaction-limited system should have a characteristic time scale of around 500 s according to eq 1. This value is comparable to the temporal change seen in Figure 4.

Irrespective of whether the sensitivity is sufficient to detect single-binding events[8] or not,[5] similar sensitivities have been previously reported. However, in contrast to other methods, the imaging mode provided by the TIRF-based readout adds another unique and attractive feature; that is that kinetics data can be obtained by analyzing residence times of single molecules in equilibrium, thus eliminating the need for time-consuming rinsing steps. To illustrate this additional feature, a kinetic analysis of fully complementary 30-mer DNA targets and DNA targets containing a single mismatch (5′-T**C**TTTCTGATGTCCAGGGTGAGACTGACGT-3′, mismatched base underlined and bold) was performed. Because each binding event can be discerned and monitored, the residence time of single vesicles can be measured and used to determine the dissociation constant, k_{off}, of the binding event. It is important to note that the assay thereby permits the kinetics information to be obtained by continuous imaging in equilibrium in contrast to conventional methods that require subsequent rinsing. To reduce statistical uncertainties, the absolute number of dissociation events was

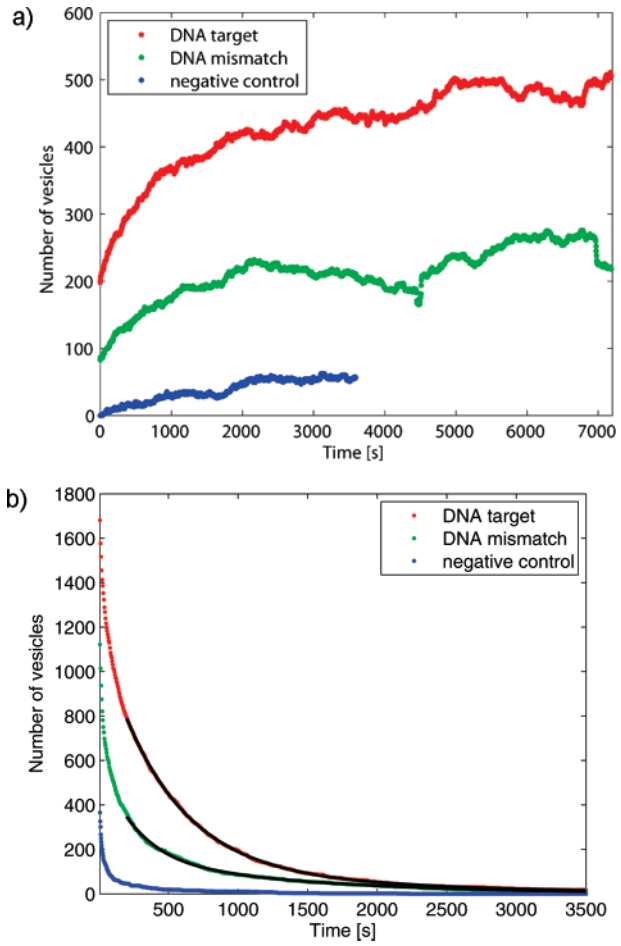

Figure 5. (a) Number of immobilized vesicles at the interface vs time in the absence of target DNA (blue), after subsequent addition of 10 pM target DNA with a single mismatch (green), and after subsequent addition of 10 pM fully complementary DNA (red). The experiment is performed in a sequential manner that eliminates the influence of surface coverage variations. Note that bleached vesicles are not counted as bound and that the measurements for target and mismatch DNA are acquired over twice as long time as the negative control experiment. (b) Curves showing the number of vesicles still attached to the surface after a certain binding time but that have lost contact with the surface before the last frame of the measurement. The black curves are curve fits ($R^2 > 0.995$ for both fits) to the DNA target and DNA mismatch data points for $t \geq 200$ s, which yields the dissociation constant describing the residence time behavior (see Supporting Information for further information). The restricted range for the curves fits is to avoid the influence of nontarget-mediated binding as seen in the negative control curve.

increased by lowering the PLL-*g*-PEG/PLL-*g*-PEGbiotin ratio to 1:100, increasing the molar ratio of DNA duplexes per vesicle to 1:2, and increasing the target concentration to 10 pM.

Figure 5a shows the number of bound vesicles in a continuous measurement starting with a negative control containing no target DNA following subsequent addition of the single mismatch DNA and finally the fully complementary target. At low DNA and vesicle concentrations (pM to fM) the surface coverage is expected to be proportional to the target concentration and inversely proportional to the equilibrium dissociation constant, K_d (see eq 1). As seen in Figure 5a, addition of fully complementary DNA results in a shift in the equilibrium coverage to a higher value reflecting the increase in binding affinity compared to the single mismatch sequence.

Even more striking is the strong contrast observed between fully complementary, single mismatch, and unspecific binding from statistics of the residence times, as seen in Figure 5b. The data clearly show that the vesicles bound in the negative control experiment are weakly bound to the surface and quickly dissociates. The residence time curves for the target and mismatch DNA show different dissociation trends, which clearly differs from each other as well as from the nonspecific interaction. Taken together, these observations demonstrate that the assay is capable of distinguishing between nonspecific interactions and different types of DNA-mediated interactions. This observation was quantified by extracting values of the dissociation constants for the target and mismatch DNA by fitting the curves to an exponential function. On the basis of the appearance of the negative control curve, influence of vesicles not bound via DNA−DNA interactions was avoided by analyzing the residence times longer than 200 s only. Furthermore, because the measurements were done over a limited time span, the number of vesicles that bind for a long time to the surface before losing contact will be lower than what will be accounted for using a pure exponential fit. An expression accounting for this behavior is derived in the Supporting Information and used for the curve fits.

Both the mismatch and target DNA curves in Figure 5b show a tail region with tightly bound vesicles. These strongly bound vesicles could arise from multiple DNA−DNA interactions between the vesicle and the surface or from irreversible binding to defects on the surface. The slow decaying tail will partly obscure the analysis of the binding kinetics of the single DNA−DNA interactions. Therefore, a double exponential fit was used to filter out the slowly varying tail region from the single DNA−DNA binding events before k_{off} was determined; see the black curves in Figure 5b for the double exponential curve fits. This yielded dissociation rate constants of 0.0020 and 0.0038 s^{-1} for target and mismatch DNA, respectively. Values on k_{off} for DNA hybridization differ significantly in the literature[1,15−17] and is a strong function of buffer composition, pH, ionic strength, and temperture.[18] However, our values on k_{off} are well within this range, but also in good agreement with previous reported relative differences in dissociation rate constants between target and a single mismatch for a 15-mer DNA strand.[17] However, we emphasize that the kinetics retrieved from the analysis should mainly serve as a demonstration of the type of information that can be extracted, while a more thorough analysis of binding kinetics is postponed to future publications.

In conclusion, the scheme developed for the detection of single DNA targets with low background offers promise for studies of single-molecule-binding dynamics in general. It could also be extended to DNA-hybridization-induced docking of laterally mobile tethered vesicles,[19] which in principle would eliminate the need of TIR excitation. The concept

could easily be extended to q-dots for which well-established biomolecular modification schemes are available. However, lipid vesicles offer the advantage of being compatible with membrane-residing receptors, which means that the system can serve as a versatile tool for sensing various types of cell membrane-related biomolecular interactions. In contrast to most other single-molecule detection schemes, the imaging mode also offers possibilities for multiple spots to be measured simultaneously in an array-based design. Array-based single nucleotide polymorphism analysis as well as screening assays for drug-candidates against membrane-residing receptors is of great importance in medical diagnostics and the pharmaceutical industry. For instance, the residence time, governed by the dissociation rate constant k_{off}, of a receptor-drug complex could provide a much better measure of the sustained drug efficacy in vivo, where the ligand concentration is not constant.[20]

Acknowledgment. This work was funded by NanoBioMaps, the SSF funded Ingvar program and the Swedish Research Council (Grant 2005-3140). We thank LayerLab AB, Göteborg, Sweden, for help with the design of the cholesterol-modified oligonucleotides.

Supporting Information Available: Filtered and nonfiltered movie sequences, materials and methods section, and image analysis in Matlab. This material is available free of charge via the Internet at http://pubs.acs.org.

References

(1) Bunimovich, Y. L.; Shin, Y. S.; Yeo, W. S.; Amori, M.; Kwong, G.; Heath, J. R. *J. Am. Chem. Soc.* **2006**, *128* (50), 16323−16331.
(2) Brousseau, L. C. *J. Am. Chem. Soc.* **2006**, *128* (35), 11346−11347.
(3) Bailey, R. C.; Nam, J. M.; Mirkin, C. A.; Hupp, J. T. *J. Am. Chem. Soc.* **2003**, *125* (44), 13541−13547.
(4) Ho, Y. P.; Kung, M. C.; Yang, S.; Wang, T. H. *Nano Lett.* **2005**, *5* (9), 1693−1697.
(5) Hahm, J.; Lieber, C. M. *Nano Lett.* **2004**, *4* (1), 51−54.
(6) Goodrich, T. T.; Lee, H. J.; Corn, R. M. *J. Am. Chem. Soc.* **2004**, *126* (13), 4086−4087.
(7) Taton, T. A.; Mirkin, C. A.; Letsinger, R. L. *Science* **2000**, *289* (5485), 1757−1760.
(8) Armani, A. M.; Kulkarni, R. P.; Fraser, S. E.; Flagan, R. C.; Vahala, K. J. *Science* **2007**, *317* (5839), 783−787.
(9) Gai, H. W.; Wang, Q.; Ma, Y. F.; Lin, B. C. *Angew. Chem., Int. Ed.* **2005**, *44* (32), 5107−5110.
(10) Jeong, S.; Park, S. K.; Chang, J. K.; Kang, S. H. *Bull. Korean Chem. Soc.* **2005**, *26* (6), 979−982.
(11) Zhao, X. J.; Tapec-Dytioco, R.; Tan, W. H. *J. Am. Chem. Soc.* **2003**, *125* (38), 11474−11475.
(12) Huang, N. P.; Voros, J.; De Paul, S. M.; Textor, M.; Spencer, N. D. *Langmuir* **2002**, *18* (1), 220−230.
(13) Stadler, B.; Falconnet, D.; Pfeiffer, I.; Hook, F.; Voros, J. *Langmuir* **2004**, *20* (26), 11348−11354.
(14) Pfeiffer, I.; Hook, F. *J. Am. Chem. Soc.* **2004**, *126* (33), 10224−10225.
(15) Howorka, S.; Movileanu, L.; Braha, O.; Bayley, H. *Proc. Natl. Acad. Sci. U.S.A.* **2001**, *98* (23), 12996−13001.
(16) Jensen, K. K.; Orum, H.; Nielsen, P. E.; Norden, B. *Biochemistry* **1997**, *36* (16), 5072−5077.
(17) Tawa, K.; Knoll, W. *Nucleic Acids Res.* **2004**, *32* (8), 2372−2377.
(18) Tan, Z. J.; Chen, S. J. *Biophys. J.* **2006**, *90* (4), 1175−1190.
(19) Chan, Y. H. M.; Lenz, P.; Boxer, S. G. *Proc. Natl. Acad. Sci. U.S.A.* **2007**, *104* (48), 18913−18918.
(20) Copeland, R. A.; Pompliano, D. L.; Meek, T. D. *Nat. Rev. Drug Discovery* **2006**, *5* (9), 730−739.

NL072401J